

**OAK RIDGE  
NATIONAL  
LABORATORY**



**Evaluation of Mixed LEU-MOX Loading  
Patterns for LWRs Originating from  
Inability to Deliver MOX Assemblies  
(Westinghouse Reload Core Study)**

**Imelda Ariani  
Paul J. Turinsky**

MANAGED AND OPERATED BY  
LOCKHEED MARTIN ENERGY RESEARCH CORPORATION  
FOR THE UNITED STATES  
DEPARTMENT OF ENERGY

This report was prepared as an account of work sponsored by an agency of the United States Government. Neither the United States Government nor any agency thereof, nor any of their employees, makes any warranty, express or implied, or assumes any legal liability or responsibility for the accuracy, completeness, or usefulness of any information, apparatus, product, or process disclosed, or represents that its use would not infringe privately owned rights. Reference herein to any specific commercial product, process, or service by trade name, trademark, manufacturer, or otherwise, does not necessarily constitute or imply its endorsement, recommendation, or favoring by the United States Government or any agency thereof. The views and opinions of authors expressed herein do not necessarily state or reflect those of the United States Government or any agency thereof.

**EVALUATION OF MIXED LEU-MOX LOADING PATTERNS FOR LWRs  
ORIGINATING FROM INABILITY TO DELIVER  
MOX ASSEMBLIES**

(Westinghouse Reload Core Study)

Imelda Ariani  
Paul J. Turinsky

Date Published: February 1999

Report Prepared by  
LOCKHEED MARTIN ENERGY RESEARCH CORP.  
P.O. Box 2008  
Oak Ridge, Tennessee 37831-6363  
under  
Subcontract Number 85B99398V

Funded by  
Office of Fissile Materials Disposition  
United States Department of Energy

Prepared for  
Computational Physics and Engineering Division  
Oak Ridge National Laboratory  
Oak Ridge, Tennessee 37831  
managed by  
LOCKHEED MARTIN ENERGY RESEARCH CORP.  
for the  
U.S. DEPARTMENT OF ENERGY  
under contract DE-96OR22464

# **FINAL REPORT**

**Evaluation of Mixed LEU-MOX Loading Patterns for LWRs**

**Originating from Inability to Deliver MOX Assemblies**

**Westinghouse Reload Core Study**

*Imelda Ariani and Paul J. Turinsky*

**Electric Power Research Center  
Department of Nuclear Engineering  
North Carolina State University  
Raleigh, NC**

**January, 1999**

---

## Contents

---

1.	Introduction.....	1
2.	Methodology .....	2
3.	Lattice Physics Predictions .....	3
4.	Equilibrium Cycle, Full MOX Core .....	3
5.	Initial Mixed LEU-MOX Core.....	15
6.	Subsequent Mixed LEU-MOX Cores .....	19
6.1	Scenario 1: MOX Feed Batches Available for Subsequent Cycle .....	20
6.2	Scenario 2: MOX Feed Batches Continue to be Unavailable for Subsequent Cycle.....	23
6.3	Transition Back to Full LEU Core.....	25
6.4	Summary of Key Core Attributes .....	27
7.	Conclusions.....	30
8.	Acknowledgment .....	30
9.	References.....	30

## List of Figures

FIGURE 1.	Equilibrium Cycle, Full MOX Core Loading Pattern.....	7
FIGURE 2.	PHOENIX/ANC vs. HELIOS/FORMOSA-P Assembly Burnup at 0.15 GWd/MTM .....	8
FIGURE 3.	PHOENIX/ANC vs. HELIOS/FORMOSA-P Assembly Power at 0.15 GWd/MTM .....	8
FIGURE 4.	PHOENIX/ANC vs. HELIOS/FORMOSA-P Peak Pin Power at 0.15 GWd/MTM .....	9
FIGURE 5.	PHOENIX/ANC vs. HELIOS/FORMOSA-P Assembly Burnup at 11 GWd/MTM .....	9
FIGURE 6.	PHOENIX/ANC vs. HELIOS/FORMOSA-P Assembly Power at 11 10	10
FIGURE 7.	PHOENIX/ANC vs. HELIOS/FORMOSA-P Peak Pin Power at 11 10	10
FIGURE 8.	PHOENIX/ANC vs. HELIOS/FORMOSA-P Assembly Burnup at 21.564 GWd/MTM .....	11
FIGURE 9.	PHOENIX/ANC vs. HELIOS/FORMOSA-P Assembly Power at 21.564 GWd/MTM .....	11
FIGURE 10.	PHOENIX/ANC vs. HELIOS/FORMOSA-P Peak Pin Power at 21.564 GWd/MTM .....	12
FIGURE 11.	PHOENIX/ANC versus HELIOS/FORMOSA-P Peak FDH .....	12
FIGURE 12.	PHOENIX/ANC versus HELIOS/FORMOSA-P Boron Coefficients.....	13
FIGURE 13.	PHOENIX/ANC versus HELIOS/FORMOSA-P MTC .....	13
FIGURE 14.	Equilibrium Cycle, Full MOX Core Key Attributes at BOC Conditions ..	14
FIGURE 15.	Equilibrium Cycle, Full MOX Core Key Attributes at EOC Conditions..	14
FIGURE 16.	Mixed Core Scenarios.....	17
FIGURE 17.	Initial Mixed Core Loading Pattern .....	18
FIGURE 18.	Initial Mixed Core Key Attributes at BOC Conditions.....	18
FIGURE 19.	Initial Mixed Core Key Attributes at EOC Conditions .....	19
FIGURE 20.	Scenario 1 Loading Pattern .....	21
FIGURE 21.	Scenario 1 Core Key Attributes at BOC Conditions.....	21
FIGURE 22.	Pin Power Distribution in Scenario 1 .....	22

---

## List of Figures

---

FIGURE 23. Scenario 1 Core Key Attributes at EOC Conditions .....	22
FIGURE 24. Scenario 2 Loading Pattern .....	23
FIGURE 25. Scenario 2 Core Key Attributes at BOC Conditions .....	24
FIGURE 26. Scenario 2 Core Key Attributes at EOC Conditions .....	24
FIGURE 27. Full LEU Core Loading Pattern .....	25
FIGURE 28. Full LEU Core Key Attributes at BOC Conditions .....	26
FIGURE 29. Full LEU Core Key Attributes at EOC Conditions .....	26
FIGURE 30. Soluble Boron Concentration vs. Cycle Burnup .....	28
FIGURE 31. Peak FDH vs. Cycle Burnup .....	28
FIGURE 32. HFP Boron Worth vs. Cycle Burnup .....	29
FIGURE 33. HFP MTC vs. Cycle Burnup .....	29

---

## List of Tables

---

TABLE 1:	Core Design and Operating Parameters.....	7
TABLE 2:	Feed Enrichment for Various Cores.....	27
TABLE 3:	Core Performance for Various Cores.....	27

## 1. Introduction

This study is in support of the weapon's grade Pu disposition project utilizing the reactor option, which entails burning weapon's grade Mixed Oxide (MOX) fuel in Light Water Reactors (LWRs). What is being evaluated is the feasibility of substituting Low Enriched Uranium (LEU) fuel assemblies for weapon's grade MOX assemblies starting from an equilibrium cycle, full MOX core. The specific focus of this report is on the Westinghouse Pressurized Water Reactor (PWR) core design, starting with an equilibrium cycle, full MOX core identified by Westinghouse [1]. The motivation for this study is two fold. Firstly, since there are technical and political uncertainties associated with the utilization of weapon's grade MOX assemblies, there is a potential that some or all of the feed fuel assemblies associated with a reload region may not be available in a timely manner. This condition will be referred to as the disruption scenario. Secondly, at the conclusion of the Pu disposition campaign, the reactors involved will need to transition back to full LEU cores. Either condition will result in the insertion of feed LEU assemblies in a core containing once and twice burnt weapon's grade MOX assemblies. There are known design challenges associated with mixed LEU-MOX cores. Work to date has addressed transitioning from an equilibrium cycle, full LEU core to an equilibrium cycle, full MOX core. The emphasis of the current study is noted to be related to the reverse transition, with the additional complexity of not knowing when this will occur for the disruption scenario.

The design features of interest include the lattice design and core loading pattern (LP). The lattice design involves the placement of fuel and burnable poison (BP) material within the fuel lattice. The lattice designs used in this study for both MOX and LEU lattices have been restricted to existing Westinghouse designs, with lattice average enrichment and BP loading as free decision variables. In determining the LP, most active LP constraints have been imposed, the exception being the shutdown margin constraint.

## 2. Methodology

To complete the mixed LEU-MOX core assessment, core simulator models must be established. This involves generating two-group, homogenized cross-sections via a lattice physics code and solving the two-group neutron diffusion equation via a core simulator code. The lattice physics code that was employed in this study is the HELIOS code [2]. HELIOS employs the Current Coupling Collision Probability (CCCP) method to solve the integral form of the neutron transport equation. The many-group cross-section library is based upon ENDF/B-VI. The resonance treatment employs the subgroup method. The core simulator that was employed is the FORMOSA-P code [3]. FORMOSA-P solves the two-dimensional (radial), two-group neutron diffusion equation utilizing the Nodal Expansion Method (NEM) based upon quartic polynomials. The microscopic depletion option of FORMOSA-P has been utilized to better represent interfacial effects at LEU-MOX assembly interfaces. Pin-power reconstruction is completed utilizing intra-nodal fluxes and pin-power form factors, correcting for spatially dependent, spectral history effects. Pin burnups are evaluated based solely upon the intra-nodal burnup distribution. The unique feature of FORMOSA-P is the incorporation of a mathematical optimization capability to determine the near-optimum LPs for a stated objective function within imposed constraints. This is done utilizing the simulated annealing, stochastic optimization method and adaptive penalty functions. In determining the LP, the feed enrichment and BP loadings of the feed assemblies are also determined to satisfy cycle energy requirement and maximum soluble boron limit, respectively. The objective utilized throughout most of this study is the minimization of the feed enrichment of the dominant feed batch, this objective function being a surrogate for minimizing the feed region cost.

To link HELIOS to FORMOSA-P, the ZENITH [2] and FORCIP-P [4] codes were employed. ZENITH can read and process the output files of HELIOS as directed by user input provided in a higher level language, *e.g.* mathematical formulas. FORCIP-P was modified to read the ZENITH output file, manipulate the cross-sections to the form required by FORMOSA-P, and create the FORMOSA-P cross-section input file.

### 3. Lattice Physics Predictions

Lattice physics calculations for fuel and non-fuel lattices were completed by the team from Texas A&M University utilizing HELIOS/ZENITH codes. HELIOS lattice physics calculations were completed for a range of MOX and LEU lattice designs, spanning different fuel enrichments and BP loadings. This provided the lattice design inventory from which FORMOSA-P selected, with fuel enrichment treated as a continuous decision variable and BP loading as an integer decision variable. For MOX assemblies, Wet Annular Burnable Absorber (WABA) rods were employed; whereas, for LEU assemblies Integral Fuel Burnable Absorber (IFBA) were employed. This was done to avoid using integral burnable absorber in MOX pins, a restriction placed on the design by DOE due to lack of burnup experience for such a configuration. For each lattice design, the lattice was depleted to high burnup at base case conditions, *i.e.* Hot Full Power (HFP) average moderator density and fuel temperature. Multiple instantaneous branch cases were executed during the depletion, enabling characterization of the cross-sections as a function of moderator density, fuel temperature and soluble boron concentration within FORMOSA-P in order to apply spatially dependent, feedback corrections.

### 4. Equilibrium Cycle, Full MOX Core

Table 1 provides the core design and operating parameters assumed throughout this study. A FORMOSA-P model has been established for the equilibrium cycle, full MOX core identified by Westinghouse [1]. This model not only provided the starting basis to evaluate subsequent reload cores, but allowed FORMOSA-P predictions of core attributes to be contrasted with those of the Westinghouse core simulator ANC for this core. Note that the cross-sections used by ANC are generated using the PHOENIX lattice physics code. An equilibrium cycle, full MOX core is established in FORMOSA-P in an iterative manner. Beginning-of-Cycle (BOC) assembly quadrant isotopics, associated with the 2x2 spatial radial mesh/assembly being employed, are initially estimated by assuming them uniform across the assembly, obtaining the isotopics from HELIOS utilizing the ANC predicted assembly average burnups. This initialization process ignores both the assembly quadrant-wise spatial dependence and core position dependent spectral history effects. In addition, equilibrium  $Sm$  conditions are initially assumed at BOC, in error since feed assemblies have no  $Sm$  and burned assemblies have peak  $Sm$ . These initialization

approximations are necessary based upon the information available. The cycle is then depleted utilizing FORMOSA-P, and BOC reestablished based upon the End-of-Cycle (EOC) isotopics and appropriate  $Sm$  conditions predicted by FORMOSA-P. This process is repeated until BOC attributes converge. For each cycle, the ANC predicted critical soluble boron values are employed, and FORMOSA-P completes a critical axial buckling search. This is necessary, since FORMOSA-P is a two-dimensional code. The implication is that contrasting ANC and FORMOSA-P predicted critical soluble boron values is meaningless. Also note that the equilibrium cycle, full MOX core identified by Westinghouse utilizes 40 w/o  $^{10}B$  isotopic abundance in the soluble boron to keep critical boron concentrations at manageable levels. Hence, all cores derived from this equilibrium cycle, full MOX core utilize 40 w/o  $^{10}B$  in the soluble boron.

The equilibrium cycle, full MOX core loading pattern is shown in Figure 1. Key core attributes as predicted by FORMOSA-P at BOC and EOC conditions are shown in Figure 14 and Figure 15, respectively. For BOC, equilibrium Xenon and peak Samarium (burnt assemblies)/ no Samarium (fresh assemblies) fission product conditions are used. All constraints are noted to be satisfied for this core, as predicted by the FORMOSA-P model.

BOC, MOC, and EOC comparisons between HELIOS/FORMOSA-P and PHOENIX/ANC of predicted core attributes are presented in Figure 2 through Figure 9. At BOC, since PHOENIX/ANC results for 0 GWd/MTM are not available, comparisons are instead presented at 0.15 GWd/MTM. Poorer agreements (compared to HELIOS/FORMOSA-P versus DIT/ROCS for the ABB-CE core) are noted. For the HELIOS/FORMOSA-P versus DIT/ROCS comparisons, we also completed a comparison between HELIOS versus DIT lattice predictions, to both assure that the HELIOS model setup was correct and predicted values are consistent. For the full MOX Westinghouse core, lattice results from PHOENIX were not available, so a comparison between HELIOS versus PHOENIX lattice predictions could not be completed. In addition, we are now contrasting a macroscopic depletion based core simulator, ANC, with a microscopic depletion based core simulator, FORMOSA-P, which may provide a reason for some of the differences observed.

Figure 2 indicates that at BOC, the burnt assemblies all have lower burnups as predicted by HELIOS/FORMOSA-P versus PHEONIX/ANC. Since an equilibrium cycle is being analyzed, further insight into the cause of the differences in BOC burnt assembly burnups can be obtained from Figure 8, which presents the EOC assembly burnup distribution. There it can be seen that the burnups of the highest burnt assemblies, *i.e.* those to be discharge, are higher and the remaining burnt assemblies, *i.e.* those to be reloaded, are lower as predicted by HELIOS/FORMOSA-P, which is to be expected since total core average assembly burnup must be preserved. Given these differences in EOC assembly burnups, one would expect that the highest and remaining burnt assemblies' powers should be lower and higher, respectively, as predicted by HELIOS/FORMOSA-P versus PHEONIX/ANC. Figure 9 indicates that this is not the case, indicating that the likely cause of the differences noted are due to HELIOS versus PHOENIX differences, *e.g.* lattice  $k_{inf}$  versus burnup curve differences, and not due to FORMOSA-P and ANC differences.

Figure 3, which presents the BOC assembly power distribution, indicates that the HELIOS/FORMOSA-P model shows an out-in radial assembly power distribution tilt versus PHOENIX/ANC. Based upon a sensitivity study completed, it is not obvious that the BOC assembly burnup distribution differences presented in Figure 2 are the source of this power distribution tilt. By EOC, the power distribution tilt has reversed to an in-out tilt due to HELIOS/FORMOSA-P under-burning the core periphery with reference to PHOENIX/ANC, which can be seen in Figure 8. Peak pin power differences at BOC, MOC and EOC are shown in Figure 4, Figure 7 and Figure 10, respectively. Figure 11 presents the radial peaking factor,  $F_{\Delta H}$ , versus cycle burnup. It can be seen that HELIOS/FORMOSA-P generally predicts lower peak pin powers than PHOENIX/ANC for the lead fuel assemblies, with differences as large as 0.05 in relative power. Much of this difference can be attributed to the difference in predicted nodal power. Again, without access to the PHOENIX results, one can only conjecture that HELIOS versus PHOENIX differences are the major source for the peak pin power prediction differences.

Figure 12 contrasts the HFP boron reactivity worths as a function of cycle burnup as predicted by HELIOS/FORMOSA-P and PHOENIX/ANC. Generally good agreement is obtained until higher cycle burnups, where now predicted boron worths differ by up to 3 pcm/ppm. The HFP moderator temperature coefficient (MTC) predicted values versus

cycle burnup are contrasted in Figure 13, where excellent agreement over the total cycle is noted.

The FORMOSA-P equilibrium cycle, full MOX core model just critiqued, provides the starting point for the mixed LEU-MOX core study.

**TABLE 1: Core Design and Operating Parameters**

Parameter	Value
Number of Fuel Assemblies	193
Fuel Lattice	17x17
Fuel Rods / Assembly	264
Active Fuel Height (in.)	144
Power Level (MWth)	3565
HFP Core Average Linear Power Density (kW/ft.)	5.68
HFP Core Power Density (kW/l)	109.21
HFP Moderator Inlet Temperature (°F)	556.6
HFP Core Average Temperature Rise (°F)	59.6
Core Loading (MTM)	81.6
Number of Feed Assemblies	92
Target Cycle Length (MWd/MTM)	21,564
Pin Discharge Burnup Limit (MWd/MTM)	60,000
Assembly Discharge Burnup Limit (MWd/MTM)	57,000
Region Discharge Burnup Limit (MWd/MTM)	45,000
Peak $F_{\Delta H}$ Limit	1.528

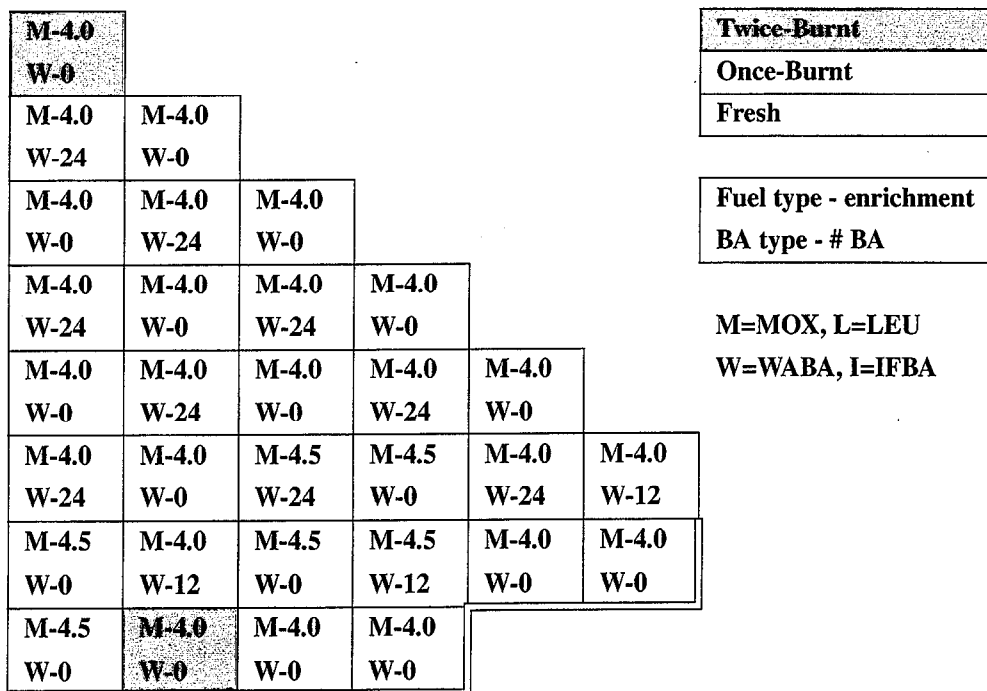


**FIGURE 1. Equilibrium Cycle, Full MOX Core Loading Pattern**

35.664 35.322 0.342			PHOENIX/ANC HELIOS/FORMOSA-P Difference		
0.175    24.743			Twice-Burnt MOX		
0.176    24.500			Once-Burnt MOX		
-0.001    0.243			Fresh MOX		
26.687    0.180    26.527			unit = GWD/MTM		
26.321    0.181    26.231					
0.366    -0.001    0.296					
0.181    27.005    0.185			24.753		
0.181    26.692    0.186			24.511		
0.000    0.313    0.001			0.242		
26.922    0.184    26.899			0.191    20.832		
26.603    0.183    26.585			0.192    20.665		
0.319    0.001    0.314			-0.001    0.167		
0.184    23.670    0.188			22.285    0.179    0.151		
0.182    23.428    0.186			22.049    0.182    0.155		
0.002    0.242    0.002			0.236    -0.005    -0.004		
16.524    0.166    26.889			0.160    0.140    27.004		
16.184    0.163    26.543			0.160    0.142    26.708		
0.340    0.003    0.346			0.000    -0.002    0.296		
0.113    29.902    18.726			27.066		
0.107    29.457    18.512			26.775		
0.006    0.445    0.214			0.291		

FIGURE 2. PHOENIX/ANC vs. HELIOS/FORMOSA-P Assembly Burnup at 0.15 GWd/MTM

0.921 0.934 -0.13			PHOENIX/ANC HELIOS/FORMOSA-P Difference		
1.171    1.062					
1.176    1.089					
-0.005    -0.027					
1.051    1.202    1.069					
1.078    1.209    1.098					
-0.027    -0.007    -0.029					
1.205    1.061    1.228			1.122		
1.209    1.087    1.233			1.146		
-0.004    -0.026    -0.005			-0.024		
1.069    1.222    1.088			1.266    1.162		
1.087    1.219    1.108			1.266    1.176		
-0.018    0.007    -0.020			0.000    -0.014		
1.227    1.087    1.246			1.169    1.181    0.997		
1.214    1.090    1.234			1.176    1.190    1.011		
0.013    -0.003    0.012			-0.007    -0.009    -0.014		
1.101    1.114    0.907			1.062    0.931    0.427		
1.072    1.096    0.906			1.054    0.926    0.422		
0.029    0.018    0.001			0.008    0.005    0.005		
0.766    0.485    0.471			0.363		
0.728    0.458    0.444			0.348		
0.038    0.027    0.027			0.015		

FIGURE 3. PHOENIX/ANC vs. HELIOS/FORMOSA-P Assembly Power at 0.15 GWd/MTM

<b>0.972</b>						PHOENIX/ANC HELIOS/FORMOSA-P Difference
<b>0.976</b>						
<b>-0.004</b>						
1.308	1.141					
1.297	1.154					
0.011	-0.013					
1.128	1.332	1.154				
1.143	1.325	1.171				
-0.016	0.008	-0.017				
1.332	1.143	1.372	1.232			
1.323	1.155	1.361	1.239			
0.009	-0.012	0.011	-0.007			
1.150	1.349	1.178	1.397	1.268		
1.154	1.333	1.185	1.390	1.280		
-0.004	0.016	-0.007	0.007	-0.012		
1.347	1.177	1.424	1.257	1.372	1.288	
1.333	1.184	1.400	1.264	1.353	1.292	
0.014	-0.007	0.024	-0.007	0.020	-0.004	
1.294	1.311	1.078	1.314	1.297	0.767	
1.279	1.299	1.073	1.317	1.322	0.784	
0.015	0.012	0.005	-0.003	-0.025	-0.017	
1.065	<b>0.750</b>	0.783	0.601			
1.040	<b>0.692</b>	0.730	0.600			
0.025	<b>0.058</b>	0.053	0.001			

FIGURE 4. PHOENIX/ANC vs. HELIOS/FORMOSA-P Peak Pin Power at 0.15 GWd/MTM

<b>46.075</b>						PHOENIX/ANC HELIOS/FORMOSA-P Difference
<b>46.013</b>						
<b>0.062</b>						
13.251	36.541					
13.251	36.662					
0.000	-0.121					
38.343	13.482	38.285				
38.347	13.503	38.380				
-0.004	-0.021	-0.095				
13.464	38.675	13.609	36.861			
13.462	38.725	13.606	36.959			
0.002	-0.050	0.003	-0.098			
38.605	13.527	38.685	13.769	33.121		
38.604	13.477	38.694	13.703	33.111		
0.001	0.050	-0.009	0.066	0.010		
13.454	35.425	13.635	34.673	12.581	10.582	
13.337	35.358	13.493	34.556	12.467	10.461	
0.117	0.067	0.142	0.117	0.114	0.121	
28.326	12.119	36.852	11.400	9.735	31.681	
27.875	11.935	36.564	11.205	9.488	31.269	
0.451	0.184	0.288	0.195	0.247	0.412	
8.430	<b>35.441</b>	24.193	31.232			
8.078	<b>34.790</b>	23.754	30.800			
0.352	<b>0.651</b>	0.439	0.432			

Unit = GWd/MTM

FIGURE 5. PHOENIX/ANC vs. HELIOS/FORMOSA-P Assembly Burnup at 11 GWd/MTM

<b>0.989</b>						
<b>1.008</b>						
<b>-0.019</b>						
1.244	1.103					
1.224	1.125					
0.020	-0.022					
1.089	1.258	1.093				
1.113	1.239	1.119				
-0.024	0.019	-0.026				
1.252	1.084	1.258	1.110			
1.234	1.110	1.242	1.136			
0.018	-0.025	0.016	-0.026			
1.078	1.246	1.082	1.255	1.111		
1.104	1.230	1.110	1.240	1.127		
-0.025	0.016	-0.027	0.015	-0.016		
1.223	1.070	1.240	1.117	1.131	0.946	
1.210	1.090	1.225	1.133	1.122	0.941	
0.013	-0.020	0.015	-0.016	0.010	0.005	
1.060	1.083	0.913	1.016	0.853	0.435	
1.063	1.074	0.926	1.007	0.844	0.433	
-0.003	0.009	-0.013	0.009	0.009	0.002	
0.753	<b>0.519</b>	0.518	0.393			
0.738	<b>0.511</b>	0.507	0.391			
0.015	<b>0.008</b>	0.011	0.002			

PHOENIX/ANC  
HELIOS/FORMOSA-P  
Difference

FIGURE 6. PHOENIX/ANC vs. HELIOS/FORMOSA-P Assembly Power at 11 GWd/MTM

<b>1.033</b>						
<b>1.044</b>						
<b>-0.011</b>						
1.315	1.174					
1.286	1.176					
0.029	-0.002					
1.155	1.318	1.156				
1.163	1.301	1.169				
-0.008	0.017	-0.013				
1.315	1.149	1.318	1.186			
1.295	1.159	1.303	1.196			
0.020	-0.010	0.015	-0.010			
1.142	1.312	1.150	1.318	1.193		
1.154	1.291	1.163	1.306	1.190		
-0.012	0.021	-0.013	0.012	0.003		
1.295	1.149	1.361	1.191	1.266	1.178	
1.278	1.166	1.326	1.202	1.234	1.170	
0.017	-0.017	0.035	-0.011	0.032	0.008	
1.227	1.233	1.061	1.224	1.151	0.728	
1.232	1.226	1.066	1.208	1.148	0.738	
-0.005	0.007	-0.005	0.016	0.003	-0.010	
1.022	<b>0.743</b>	0.807	0.632			
1.003	<b>0.728</b>	0.777	0.630			
0.019	<b>0.015</b>	0.030	0.002			

PHOENIX/ANC  
HELIOS/FORMOSA-P  
Difference

FIGURE 7. PHOENIX/ANC vs. HELIOS/FORMOSA-P Peak Pin Power at 11 GWd/MTM

<b>56.629</b>						
<b>56.705</b>						
<b>-0.076</b>						
26.530	48.152					
26.195	48.467					
0.335	-0.315					
49.807	26.846	49.762				
50.015	26.576	50.099				
-0.208	0.270	-0.337				
26.762	50.068	26.940	48.468			
26.483	50.353	26.689	48.847			
0.279	-0.285	0.251	-0.379			
49.920	26.736	50.021	27.012	44.714		
50.174	26.453	50.317	26.764	44.926		
-0.254	0.283	-0.296	0.248	-0.212		
26.367	46.612	26.754	46.303	24.585	20.657	
26.089	46.797	26.429	46.430	24.341	20.460	
0.278	-0.185	0.325	-0.127	0.244	0.197	
39.345	23.507	46.502	22.109	18.657	36.396	
39.023	23.259	46.390	21.854	18.416	35.988	
0.322	0.248	0.112	0.255	0.241	0.408	
16.360	<b>41.057</b>	29.831	35.528			
15.959	<b>40.358</b>	29.294	35.094			
0.401	<b>0.699</b>	0.537	0.434			

PHOENIX/ANC  
HELIOS/FORMOSA-P  
Difference

Unit = GWd/MTM

FIGURE 8. PHOENIX/ANC vs. HELIOS/FORMOSA-P Assembly Burnup at 21.564 GWd/MTM

<b>1.004</b>						
<b>1.008</b>						
<b>-0.004</b>						
1.256	1.091					
1.213	1.099					
0.043	-0.008					
1.078	1.260	1.078				
1.088	1.220	1.091				
-0.010	0.040	-0.013				
1.255	1.071	1.256	1.088			
1.217	1.085	1.221	1.105			
0.038	-0.014	0.035	-0.016			
1.065	1.247	1.065	1.246	1.087		
1.083	1.216	1.086	1.221	1.102		
-0.018	0.031	-0.021	0.025	-0.015		
1.219	1.053	1.241	1.089	1.139	0.962	
1.199	1.071	1.217	1.109	1.124	0.958	
0.020	-0.018	0.024	-0.020	0.015	0.004	
1.036	1.079	0.921	1.017	0.841	0.460	
1.053	1.074	0.941	1.015	0.857	0.479	
-0.017	0.005	-0.020	0.002	-0.016	-0.019	
0.757	<b>0.550</b>	0.555	0.423			
0.773	<b>0.563</b>	0.564	0.443			
-0.016	<b>-0.013</b>	-0.009	-0.020			

PHOENIX/ANC  
HELIOS/FORMOSA-P  
Difference

FIGURE 9. PHOENIX/ANC vs. HELIOS/FORMOSA-P Assembly Power at 21.564 GWd/MTM

PHOENIX/ANC HELIOS/FORMOSA-P Difference					
1.046					
1.038					
0.008					
1.302	1.150				
1.252	1.136				
0.050	0.014				
1.137	1.303	1.133			
1.127	1.256	1.127			
0.010	0.047	0.006			
1.298	1.130	1.299	1.144		
1.252	1.122	1.257	1.147		
0.046	0.008	0.042	-0.003		
1.125	1.291	1.127	1.295	1.155	
1.120	1.251	1.125	1.261	1.152	
0.005	0.040	0.002	0.034	0.003	
1.277	1.120	1.321	1.157	1.248	1.174
1.243	1.128	1.272	1.160	1.218	1.154
0.034	-0.008	0.049	-0.003	0.030	0.020
1.177	1.212	1.042	1.195	1.106	0.740
1.186	1.193	1.054	1.180	1.106	0.758
-0.008	0.019	-0.012	0.015	0.000	-0.018
1.014	0.761	0.821	0.664		
1.001	0.760	0.814	0.671		
0.013	0.001	0.006	-0.007		

FIGURE 10. PHOENIX/ANC vs. HELIOS/FORMOSA-P Peak Pin Power at 21.564 GWd/MTM

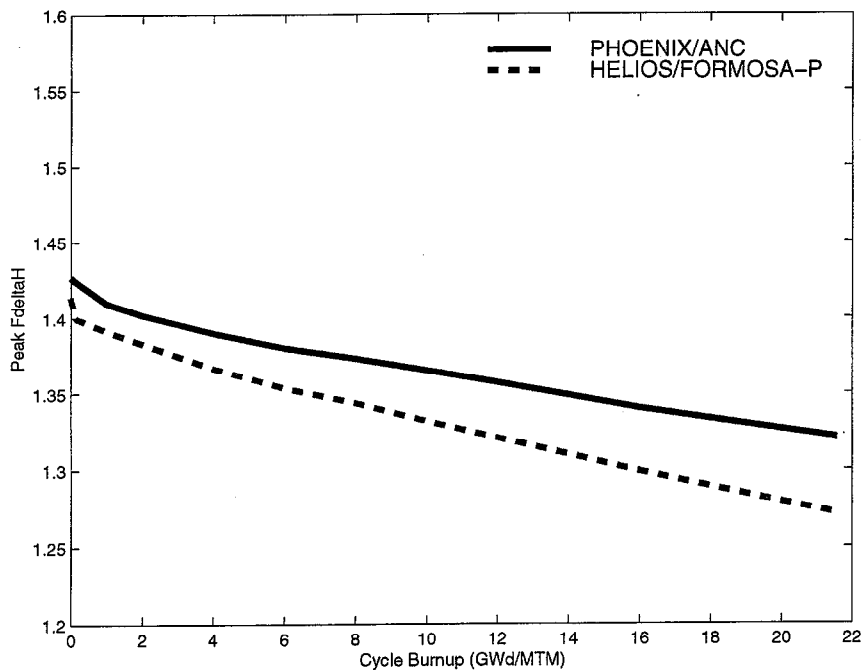
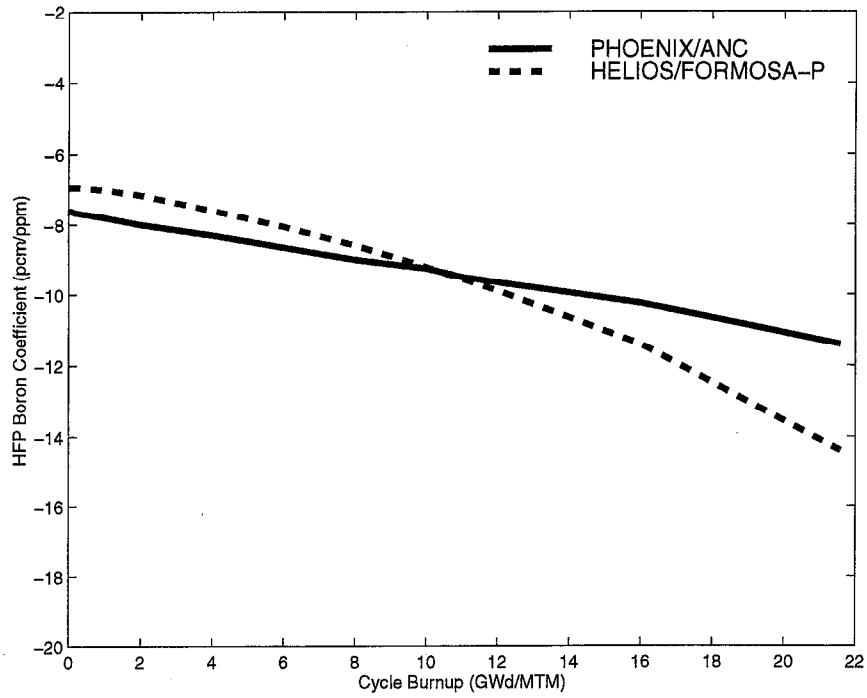
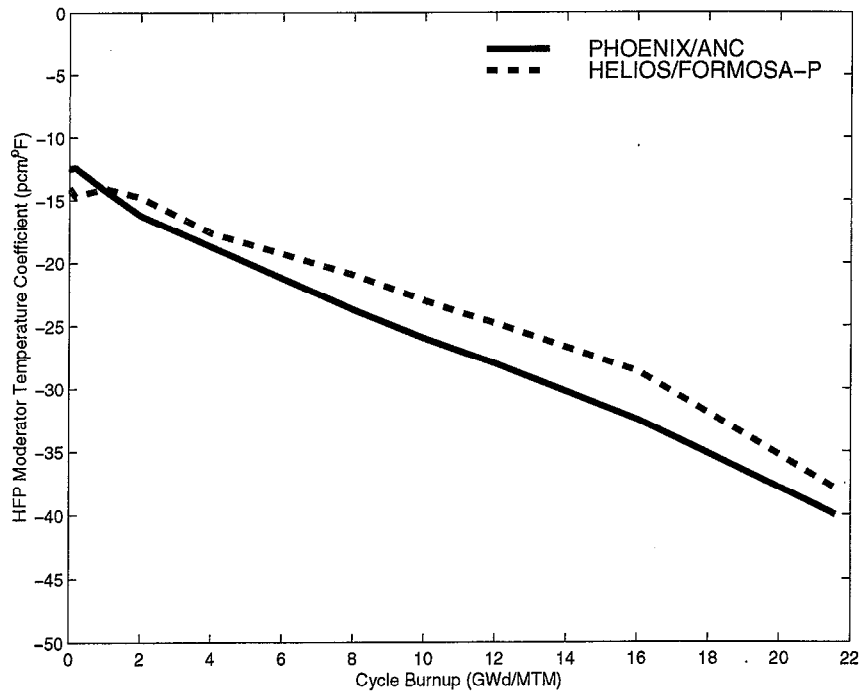


FIGURE 11. PHOENIX/ANC versus HELIOS/FORMOSA-P Peak  $F_{\Delta H}$



**FIGURE 12. PHOENIX/ANC versus HELIOS/FORMOSA-P Boron Coefficients**



**FIGURE 13. PHOENIX/ANC versus HELIOS/FORMOSA-P MTC**

<b>35.18</b>					
<b>0.922</b>					
<b>0.963</b>					
0.000	24.34				
1.173	1.077				
1.289	1.141				
26.16	0.000	26.07			
1.067	1.209	1.090			
1.132	1.328	1.163			
0.000	26.53	0.000	24.34		
1.209	1.078	1.238	1.145		
1.326	1.146	1.360	1.239		
26.44	0.000	26.42	0.000	20.49	
1.077	1.221	1.104	1.281	1.185	
1.142	1.340	1.182	<b>1.414</b>	1.293	
0.000	23.27	0.000	21.87	0.000	0.000
1.212	1.080	1.240	1.180	1.217	1.036
1.336	1.171	1.410	1.271	1.372	1.328
16.03	0.000	26.41	0.000	0.000	26.64
1.056	1.089	0.896	1.064	0.946	0.426
1.262	1.296	1.067	1.337	1.355	0.800
0.000	<b>29.39</b>	18.45	26.72		
0.715	<b>0.446</b>	0.433	0.343		
1.026	<b>0.679</b>	0.715	0.595		

Assembly Burnup (GWd/MTM)  
 Assembly Power  
 Peak Pin Power  
**Twice-Burnt MOX**  
 Once-Burnt MOX  
 Fresh MOX

**bold** denotes maximum value

**FIGURE 14. Equilibrium Cycle, Full MOX Core Key Attributes at BOC Conditions**

<b>56.70</b>					
<b>1.008</b>					
<b>57.27</b>					
26.19	48.47				
1.213	1.099				
27.97	49.87				
50.02	26.58	50.10			
1.088	1.220	1.091			
50.21	28.14	50.37			
26.48	50.35	26.69	48.85		
1.217	1.085	1.221	1.105		
28.06	50.42	28.29	50.06		
50.17	26.45	50.32	26.76	44.93	
1.083	1.216	1.086	1.221	1.102	
50.19	28.10	50.54	28.34	48.94	
26.09	46.80	26.43	46.43	24.34	20.46
1.199	1.071	1.217	1.109	1.124	0.958
27.83	49.16	29.76	50.72	27.19	25.62
39.02	23.26	46.39	21.85	18.42	35.99
1.053	1.074	0.941	1.015	0.857	0.479
41.49	26.68	51.41	26.87	24.69	44.53
15.96	<b>40.36</b>	29.30	35.10		
0.773	<b>0.563</b>	0.564	0.443		
22.98	<b>45.71</b>	31.29	42.16		

Assembly Burnup (GWd/MTM)  
 Assembly Power  
 Peak Pin Burnup (GWd/MTM)  
**Thrice-Burnt MOX**  
 Twice-Burnt MOX  
 Once-Burnt MOX

**bold** denotes maximum value

**FIGURE 15. Equilibrium Cycle, Full MOX Core Key Attributes at EOC Conditions**

## 5. Initial Mixed LEU-MOX Core

Several scenarios (Figure 16) were examined in regard to mixed LEU-MOX cores starting with the equilibrium cycle, full MOX core. All scenarios have in common that the first cycle that LEU feed assemblies are loaded into the core, all MOX feed assemblies are unavailable and replaced by LEU feed assemblies. This will be referred to as the Initial Mixed LEU-MOX Core. In subsequent cycles, different scenarios are assumed depending upon the availability of MOX feed assemblies, as will be described in Section 6. For all scenarios, the LEU lattice designs used are the standard Westinghouse LEU lattice designs with uniform pin-wise enrichment distribution. The MOX lattice designs used in this study are also assumed to have uniform pin-wise enrichment distribution. As noted earlier, the LEU assemblies utilize IFBAs while MOX assemblies utilize WABAs as burnable absorbers.

For the initial mixed LEU-MOX core, the following design approach was employed. First, the non-dominant MOX feed batch, *i.e.* smaller size feed batch, is replaced by an LEU feed batch to find the “equivalent” LEU feed batch whose BP loading and  $^{235}\text{U}$  enrichment produce the same cycle energy production and maximum soluble boron concentration for the first cycle loaded, utilizing the minimum non-dominant batch feed enrichment possible. In completing this assessment of the lattice attributes of the non-dominant LEU feed batch, the core LP is fixed and dominant MOX feed batch retained, with the only constraints imposed being those noted above, *i.e.* cycle energy requirement and maximum soluble boron concentration. This assessment is completed utilizing FORMOSA-P without automatic optimization capability activated. Using this approach, the non-dominant feed batch enrichment is determined to be 4.0 w/o  $^{235}\text{U}$ .

Fixing the non-dominant LEU feed batch at the equivalent feed batch attributes, the dominant LEU feed batch is determined such that the cycle energy requirement (21,564 MWd/MTM) and all constraints [maximum soluble boron concentration (1,829 ppm), radial pin-wise power peaking (1.528), maximum pin-wise discharge burnup (60 GWd/MTHM), maximum assembly discharge burnup (57 GWd/MTM), and maximum region discharge burnup (45 GWd/MTM)] are satisfied and the dominant LEU feed batch enrichment is minimized. This is accomplished utilizing FORMOSA-P with the automatic optimization capability activated. During optimizations, fresh assemblies locations are

fixed to their original locations (as in the equilibrium cycle, full MOX core) while burnt assemblies are allowed to shuffle. BP loadings for both minor and major feed batches are determined via FORMOSA-P optimizations. The number of BPs available for selections are 0, 16, 48, 64, 80, 104, and 128 IFBA rods per assembly. The major feed batch enrichment determined by FORMOSA-P is 3.5 w/o  $^{235}\text{U}$ . The initial mixed core loading pattern is shown in Figure 17, and some key core attributes at BOC and EOC conditions are shown in Figure 18 and Figure 19, respectively. The maximum pin power is found to be 1.518, higher than the maximum value for the full MOX core, but within the limit imposed of 1.528. The maximum pin power occurs in a once-burnt MOX assembly in a pin located on the edge of the assembly whose surface is adjacent to a fresh LEU assembly. Apparently, thermal neutron diffusion from the LEU to MOX assembly, caused by the much softer energy spectrum in the LEU assembly, is causing the power peaking in the adjacent MOX assembly. All the other constraints imposed are satisfied.

The resulting LP for the initial mixed LEU-MOX core is the starting point for the optimization of subsequent cycles as now explained.

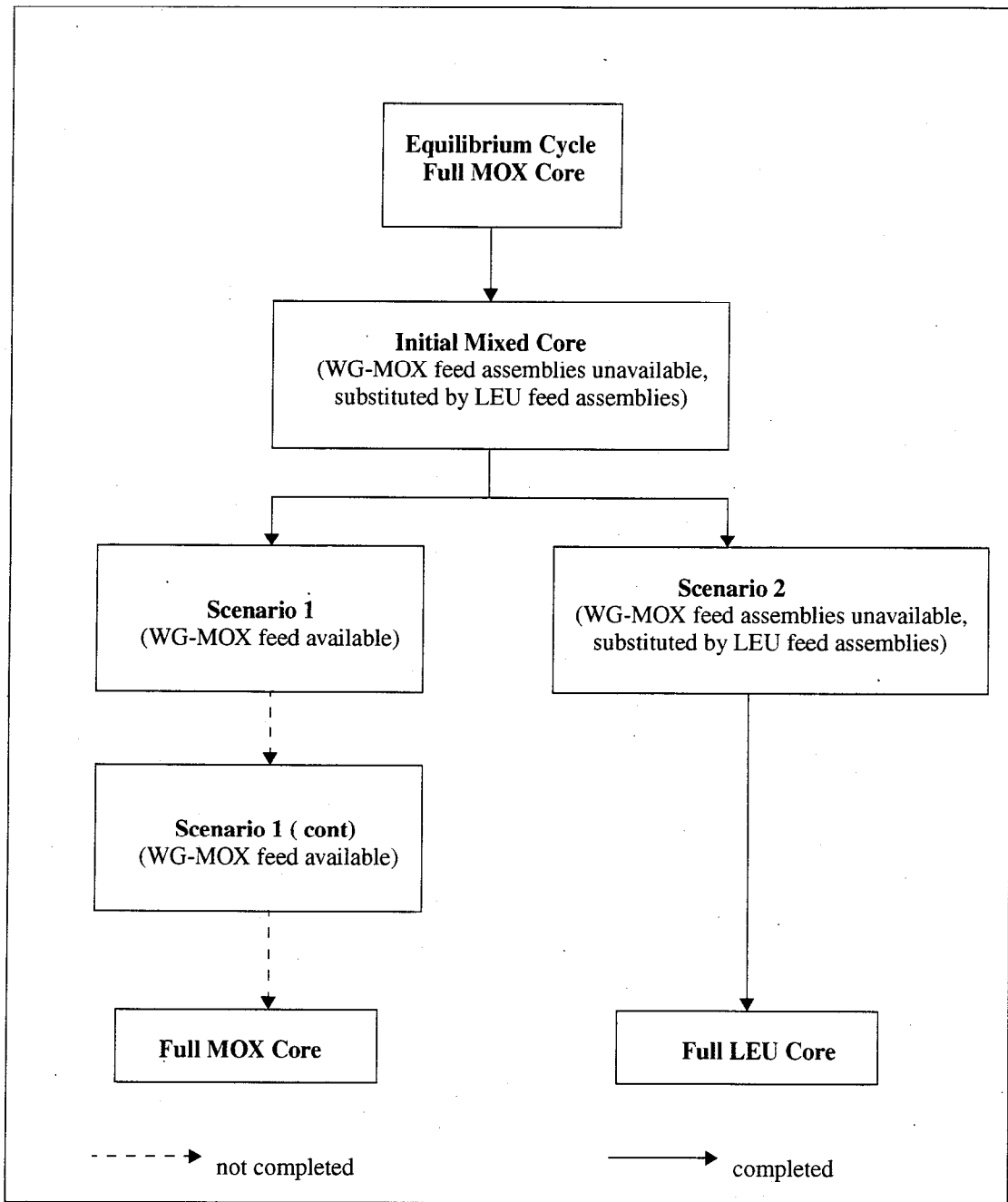


FIGURE 16. Mixed Core Scenarios

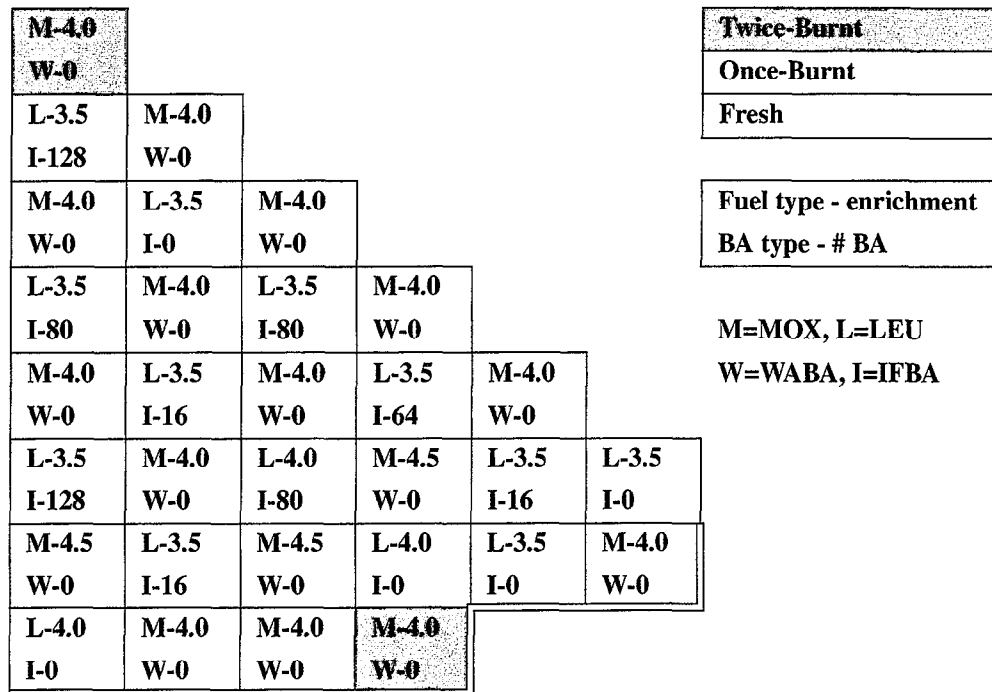


FIGURE 17. Initial Mixed Core Loading Pattern

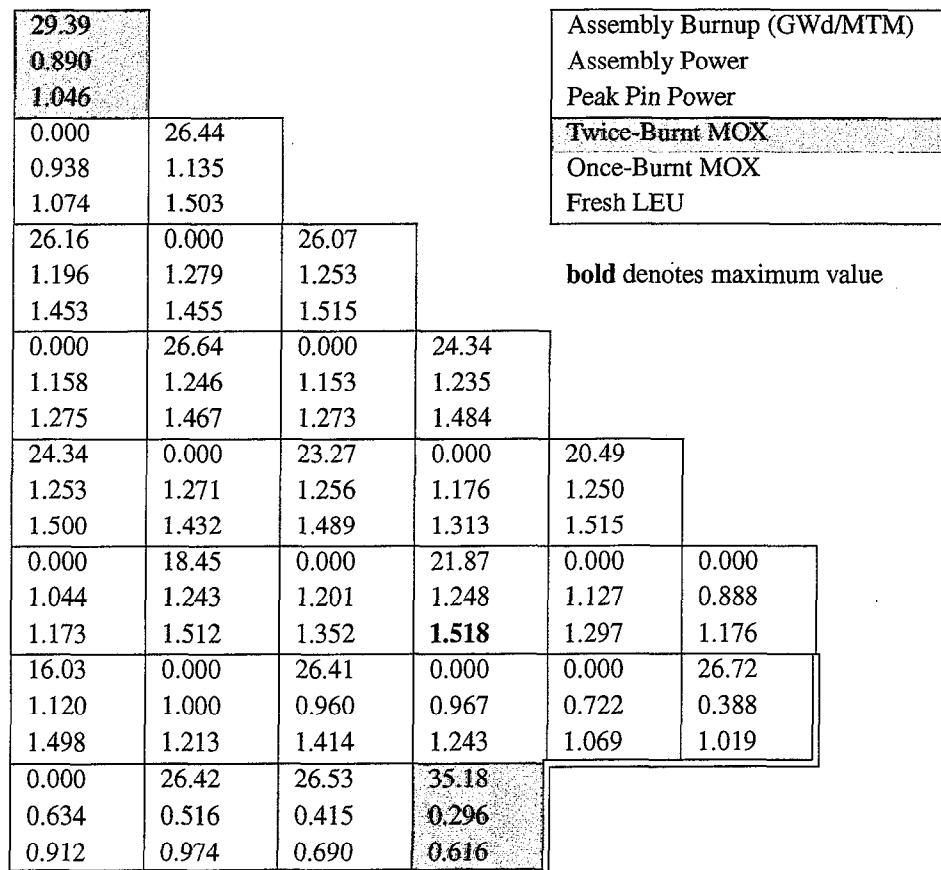


FIGURE 18. Initial Mixed Core Key Attributes at BOC Conditions

<b>51.45</b>					
<b>1.041</b>					
<b>56.75</b>					
24.52	50.52				
1.160	1.075				
26.86	58.67				
50.58	25.98	50.91			
1.074	1.139	1.075			
58.26	28.55	58.62			
25.76	51.42	26.01	49.83		
1.149	1.073	1.159	1.111		
28.17	59.11	28.50	57.07		
49.73	26.52	48.85	26.30	45.83	
1.104	1.163	1.114	1.184	1.136	
57.80	29.15	57.78	28.99	53.44	
25.54	44.13	26.95	47.46	24.17	19.61
1.182	1.137	1.225	1.158	1.155	1.001
28.05	55.94	29.77	60.00	27.25	24.90
40.07	22.31	46.94	20.97	16.37	35.86
1.117	1.066	0.976	1.033	0.865	0.515
50.92	26.34	58.20	25.47	23.12	50.60
14.87	38.30	36.25	<b>42.25</b>		
0.785	0.622	0.525	<b>0.402</b>		
20.12	50.80	43.42	<b>56.10</b>		

Assembly Burnup (GWd/MTM)
Assembly Power
Peak Pin Burnup (GWd/MTM)
<b>Thrice-Burnt MOX</b>
Twice-Burnt MOX
Once-Burnt LEU

**bold** denotes maximum value

FIGURE 19. Initial Mixed Core Key Attributes at EOC Conditions

## 6. Subsequent Mixed LEU-MOX Cores

Starting with the initial mixed core defined in Section 5, two scenarios (see Figure 16) are introduced in regard to availability of MOX feed assemblies in the subsequent cycle: (1) assume that MOX feed batches are available and (2) assume that MOX feed batches continue to be unavailable. LEU lattice designs are limited to standard Westinghouse designs which employ uniform pin-wise enrichment distributions. MOX lattice designs are limited to MOX designs used in the Westinghouse equilibrium cycle full MOX core, which also employ uniform pin-wise enrichment distributions. This was done to determine if acceptable LPs could be determined without the need to develop new and more complex lattice designs.

## 6.1 Scenario 1: MOX Feed Batches Available for Subsequent Cycle

MOX feed batch attributes are determined using FORMOSA-P optimizations in manners similar to determining the feed batch attributes for the initial mixed core. The objective of FORMOSA-P optimizations is to minimize the major feed batch enrichment. As before, during optimizations, fresh assembly locations are fixed to their original locations (as in the equilibrium cycle, full MOX core) while burnt assemblies are allowed to shuffle. BP loadings for both minor and major feed batches are also determined via FORMOSA-P optimizations using the WABA designs.

Currently, we have not found a loading pattern which satisfies the maximum pin power limit, with numerous violations occurring. As mentioned before, the MOX lattice designs employed are limited to the MOX designs used in the Westinghouse equilibrium cycle, full MOX core. The designs employ uniform pin-wise enrichment distribution. Figure 21 and Figure 22 show that when a fresh MOX assembly is adjacent to a once-burnt LEU assembly, pin powers for the pins in the outer rows of the MOX assembly are very high relative to the assembly average power. This suggests that pin-wise enrichment zoning might be necessary to control the peak pin power. Indeed, this was the approach taken by Westinghouse during the transition cycles from a full LEU core to full MOX core. Note that the discharge burnup (Figure 23) and boron concentration limits for this scenario are already satisfied. The feed enrichments determined (Figure 20) should be acceptable with regard to criticality limitations. Reemploying FORMOSA-P and removing the restriction of freezing the fresh assemblies locations at their original locations did not result in any reduction in the peak pin power.

<b>M-4.0</b>						
<b>W-0</b>						
M-4.4	L-3.5					
W-24	I-0					
L-3.5	M-4.4	L-3.5				
I-128	W-12	I-0				
M-4.4	L-3.5	M-4.4	L-3.5			
W-0	I-16	W-12	I-80			
L-3.5	M-4.4	L-3.5	M-4.4	L-3.5		
I-128	W-12	I-80	W-24	I-0		
M-4.4	L-3.5	M-4.8	L-3.5	M-4.4	M-4.4	
W-12	I-16	W-12	I-0	W-12	W-0	
L-4.0	M-4.4	L-4.0	M-4.8	M-4.4	L-3.5	
I-0	W-0	I-0	W-0	W-0	I-64	
M-4.8	L-4.0	L-3.5	<b>M-4.0</b>			
W-0	I-80	I-16	<b>W-0</b>			

<b>Twice-Burnt</b>
Once-Burnt
Fresh

Fuel type - enrichment
BA type - # BA

M=MOX, L=LEU  
W=WABA, I=IFBA

FIGURE 20. Scenario 1 Loading Pattern

36.36					
0.823					
0.863					
0.000	19.73				
1.130	0.862				
1.568	0.952				
24.46	0.000	25.91			
0.887	1.314	0.855			
0.990	<b>1.679</b>	0.920			
0.000	26.43	0.000	25.69		
1.52	0.900	1.298	0.834		
<b>1.728</b>	0.991	<b>1.630</b>	0.909		
25.48	0.000	25.92	0.000	25.91	
0.948	1.385	0.876	1.220	0.925	
1.028	<b>1.726</b>	0.968	<b>1.736</b>	1.062	
0.000	22.34	<b>0.000</b>	16.52	0.000	0.000
1.427	0.953	1.399	1.014	1.481	1.354
<b>1.745</b>	1.059	<b>1.756</b>	1.174	<b>1.746</b>	<b>1.730</b>
15.00	0.000	21.05	0.000	0.000	26.23
0.991	1.285	0.819	1.265	1.110	0.405
1.207	<b>1.715</b>	1.034	<b>1.731</b>	<b>1.565</b>	0.758
0.000	26.89	24.20	<b>35.99</b>		
0.766	0.422	0.317	<b>0.311</b>		
1.263	0.670	0.537	<b>0.587</b>		

Assembly Burnup (Gwd/MTM)
Assembly Power
Peak Pin Power
<b>Twice-Burnt MOX</b>
Once-Burnt LEU
Fresh MOX

bold denotes violations

FIGURE 21. Scenario 1 Core Key Attributes at BOC Conditions

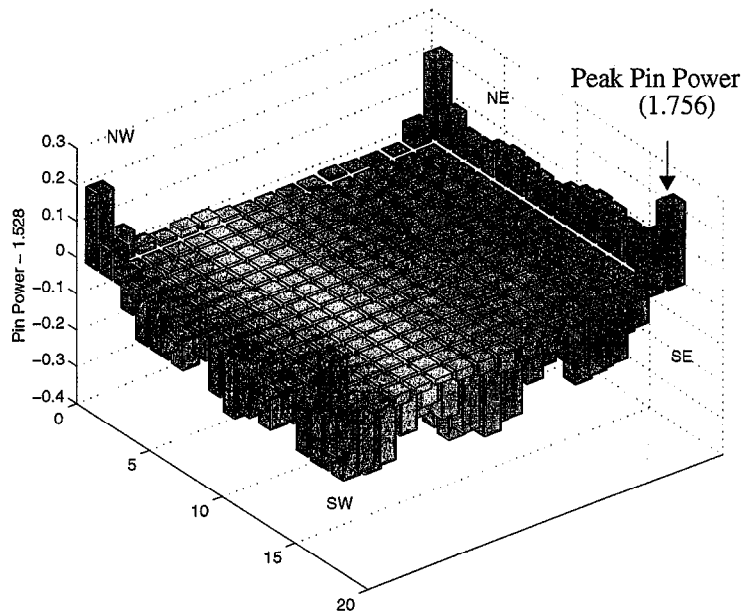


**FIGURE 22. Pin Power Distribution in Scenario 1**

*(Assembly location is shown by bold edges in Figure 21)*

<b>57.67</b>					
<b>1.020</b>					
<b>58.31</b>					
27.60	41.69				
1.293	1.034				
37.95	46.82				
45.95	29.21	46.77			
0.994	1.304	0.978			
50.36	38.90	51.27			
30.55	47.44	28.63	46.06		
1.305	0.969	1.296	0.982		
39.82	51.94	38.31	50.46		
46.91	29.14	46.65	27.08	46.17	
0.977	1.293	0.982	1.281	0.966	
51.39	38.86	51.11	37.27	50.94	
29.32	43.83	29.12	38.42	27.01	23.27
1.295	0.993	1.317	1.022	1.200	1.028
38.88	49.68	40.27	44.46	37.85	28.55
37.06	26.26	39.82	24.05	19.79	34.63
1.022	1.186	0.912	1.087	0.895	0.433
42.43	38.63	44.11	38.76	27.02	41.83
17.21	37.72	32.85	<b>43.30</b>		
0.845	0.582	0.491	<b>0.395</b>		
31.44	44.51	38.00	<b>54.41</b>		

Assembly Burnup (GWd/MTM)  
 Assembly Power  
 Peak Pin Burnup (GWd/MTM)

**Thrice-Burnt MOX**

Twice-Burnt LEU  
 Once-Burnt MOX

**FIGURE 23. Scenario 1 Core Key Attributes at EOC Conditions**

## 6.2 Scenario 2: MOX Feed Batches Continue to be Unavailable for Subsequent Cycle

For this scenario, MOX feed assemblies are assumed to continue to be unavailable and are replaced by LEU feed assemblies. Figure 24 presents the loading pattern determined by FORMOSA-P employing the objective of minimizing the major feed batch enrichment. As before, during optimizations fresh assemblies locations are fixed to their original locations (as in the equilibrium cycle, full MOX core) while burnt assemblies are allowed to shuffle. BP loadings for both minor and major feed batches are determined via the FORMOSA-P optimization using the IFBA design. The LEU enrichments for the major and minor feed batches are within the critical material limits for fuel fabrication and spent fuel pool storage (5.0 w/o  $^{235}U$ ). BOC and EOC conditions are shown in Figure 25 and Figure 26, respectively. The maximum  $F_{\Delta H}$  (1.462) is well within the limit imposed of 1.528. The maximum pin discharge burnup (59.52 GWd/MTM) is also within the limit imposed.

<b>M-4.0</b>						
<b>W-0</b>						
L-4.1	L-3.5					
I-128	I-0					
L-3.5	L-4.1	L-3.5				
I-0	I-80	I-128				
L-4.1	L-3.5	L-4.1	L-3.5			
I-80	I-16	I-80	I-128			
L-3.5	L-4.1	L-3.5	L-4.1	L-3.5		
I-80	I-80	I-16	I-104	I-0		
L-4.1	L-4.0	L-4.5	L-3.5	L-4.1	L-4.1	
I-80	I-0	I-104	I-0	I-128	I-0	
L-4.0	L-4.1	L-4.0	L-4.5	L-4.1	L-3.5	
I-0	I-80	I-80	I-0	I-0	I-16	
L-4.5	L-3.5	L-3.5	<b>M-4.0</b>			
I-0	I-80	I-64	<b>W-0</b>			

<b>Twice-Burnt</b>
<b>Once-Burnt</b>
<b>Fresh</b>

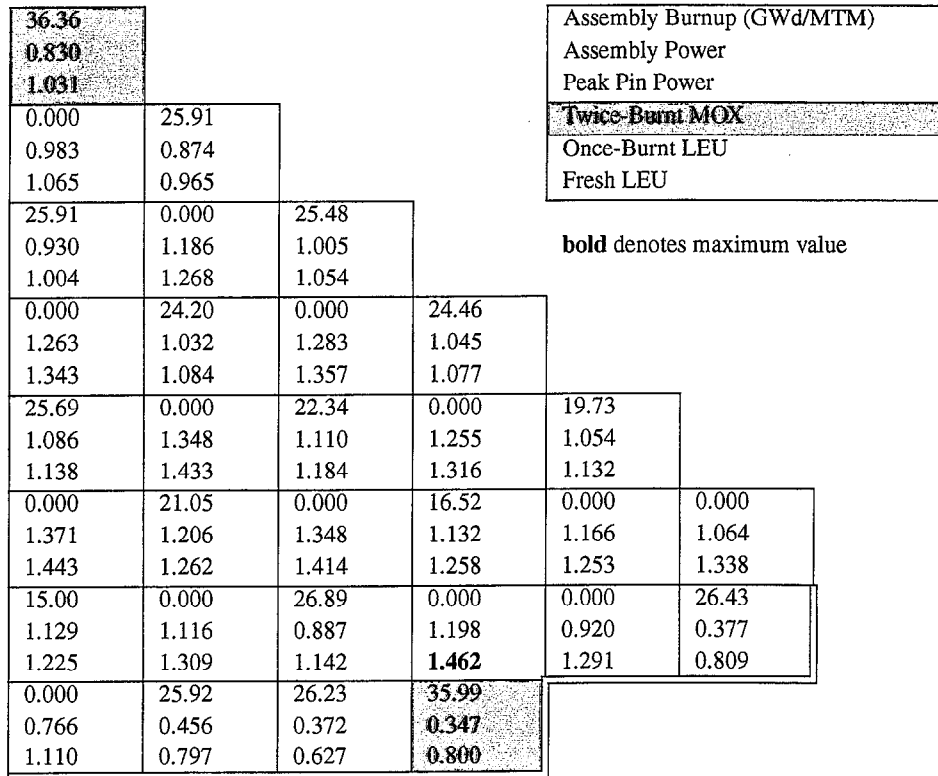
  

<b>Fuel type - enrichment</b>
<b>BA type - # BA</b>

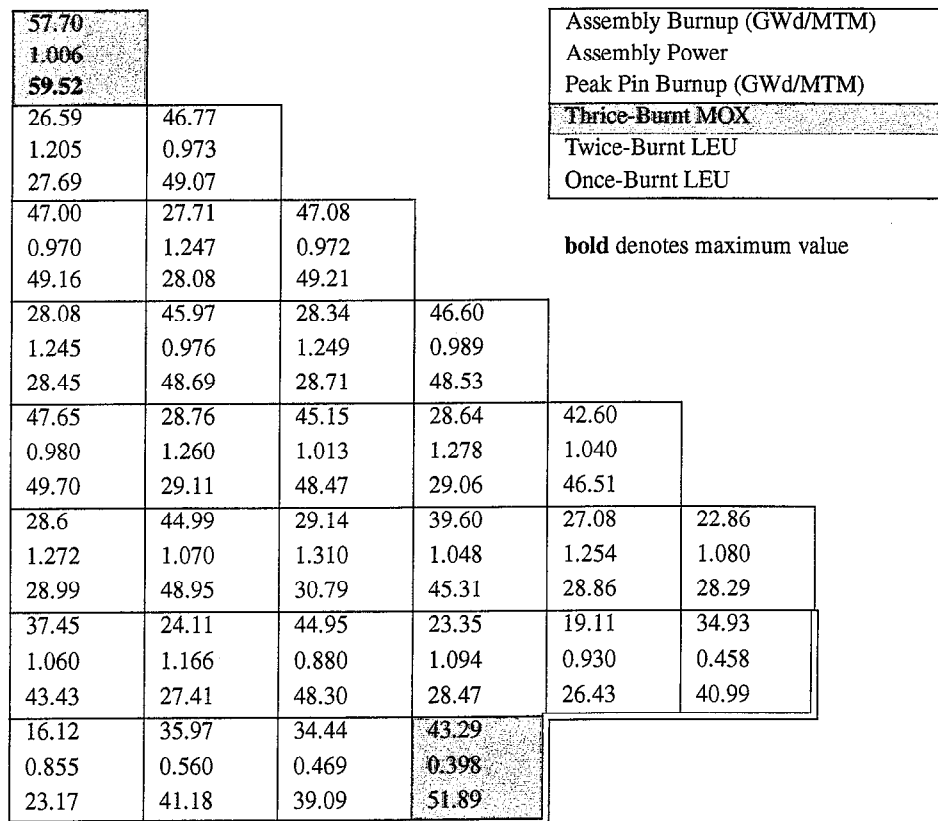
  

M=MOX, L=LEU  
W=WABA, I=IFBA

FIGURE 24. Scenario 2 Loading Pattern



**FIGURE 25. Scenario 2 Core Key Attributes at BOC Conditions**



**FIGURE 26. Scenario 2 Core Key Attributes at EOC Conditions**

### 6.3 Transition Back to Full LEU Core

Continuing Scenario 2, which assumes the unavailability of MOX feed assemblies, a transition back to a full LEU core occurs. Figure 27 presents the loading pattern determined by FORMOSA-P for this condition, employing the objective of minimizing the major feed batch enrichment. As before, during optimization, fresh assemblies locations are fixed to their original locations (as in the equilibrium cycle, full MOX core) while burnt assemblies are allowed to shuffle. BP loadings for both minor and major feed batches are determined via FORMOSA-P optimization utilizing the IFBA design. The LEU enrichments for the major and minor feed batches are well within the criticality limits. From Figure 28 and Figure 29 it can be seen that pin power and discharge burnup limits are all satisfied for the optimum LP identified by FORMOSA-P.

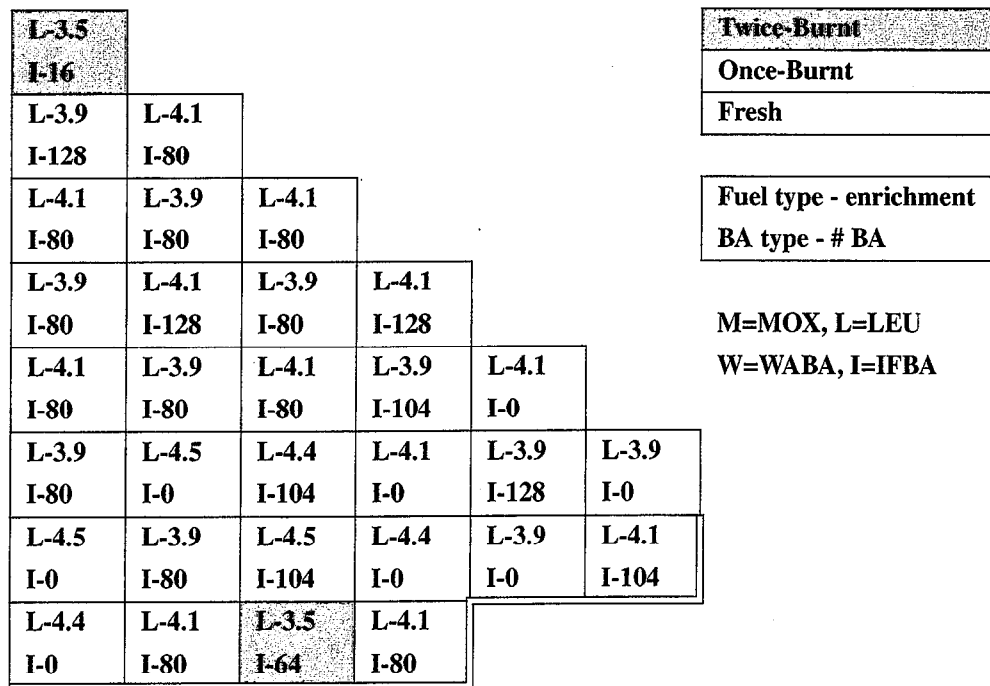


FIGURE 27. Full LEU Core Loading Pattern

<b>35.03</b>					
<b>0.638</b>					
<b>0.653</b>					
0.000	28.24				
0.909	0.872				
0.994	0.957				
28.24	0.000	27.99			
0.948	1.147	1.037			
1.019	1.240	1.095			
0.000	27.03	0.000	26.51		
1.234	1.086	1.274	1.114		
1.322	1.169	1.358	1.152		
28.54	0.000	24.16	0.000	22.88	
1.125	1.329	1.180	1.250	1.111	
1.178	1.417	1.256	1.302	1.172	
0.000	23.39	0.000	19.19	0.000	0.000
1.344	1.246	1.346	1.199	1.128	1.015
1.422	1.306	1.414	1.296	1.228	1.281
16.29	0.000	29.07	0.000	0.000	28.54
1.181	1.086	0.889	1.182	0.881	0.381
1.264	1.287	1.088	<b>1.446</b>	1.248	0.799
0.000	27.62	<b>34.58</b>	28.66		
0.771	0.472	<b>0.317</b>	0.322		
1.116	0.815	<b>0.532</b>	0.626		

Assembly Burnup (GWd/MTM)  
 Assembly Power  
 Peak Pin Power  
**Twice-Burnt LEU**  
 Once-Burnt LEU  
 Fresh LEU

FIGURE 28. Full LEU Core Key Attributes at BOC Conditions

<b>52.84</b>					
<b>0.897</b>					
<b>53.05</b>					
25.62	49.55				
1.234	1.003				
26.07	50.91				
50.00	27.13	50.30			
1.000	1.222	0.997			
51.12	27.49	51.45			
27.55	49.79	28.04	49.79		
1.217	1.007	1.223	1.023		
27.87	51.38	28.39	50.86		
51.21	28.32	48.17	28.33	46.68	
1.001	1.232	1.049	1.252	1.072	
51.58	28.80	51.00	28.65	51.69	
28.09	48.03	28.95	43.36	26.35	22.03
1.246	1.093	1.295	1.087	1.231	1.060
28.67	52.96	30.01	50.16	27.48	27.40
39.64	23.58	47.25	23.06	18.43	37.21
1.096	1.143	0.892	1.094	0.913	0.476
47.66	26.49	52.75	27.69	25.66	46.26
16.10	37.99	<b>41.72</b>	35.63		
0.852	0.579	<b>0.421</b>	0.402		
22.88	44.63	<b>48.83</b>	41.59		

Assembly Burnup (GWd/MTM)  
 Assembly Power  
 Peak Pin Burnup (GWd/MTM)  
**Thrice-Burnt LEU**  
 Twice-Burnt LEU  
 Once-Burnt LEU

**bold denotes maximum value**

FIGURE 29. Full LEU Core Key Attributes at EOC Conditions

## 6.4 Summary of Key Core Attributes

Table 2 summarizes the feed enrichments used in the various cores being studied. The feed enrichments for all cores examined satisfy the criticality limit. Soluble boron concentrations,  $F_{\Delta H}$ , HFP boron worth, and HFP MTC as a function of cycle burnup for the various cores examined are presented in Figure 30 through Figure 33. The indicated behaviors are as to be expected based upon the size and burnups of MOX and LEU batches within the core.

**TABLE 2: Feed Enrichment for Various Cores**

Core	Feed Batch Enrichment	
	20 Assemblies	72 Assemblies
Equilibrium Cycle, Full MOX	4.5 w/o WGPu	4.0 w/o WGPu
Initial Mixed Core	4.0 w/o $^{235}\text{U}$	3.5 w/o $^{235}\text{U}$
Scenario 1	4.8 w/o WGPu	4.4 w/o WGPu
Scenario 2	4.5 w/o $^{235}\text{U}$	4.1 w/o $^{235}\text{U}$
Full LEU	4.4 w/o $^{235}\text{U}$	3.9 w/o $^{235}\text{U}$

**TABLE 3: Core Performance for Various Cores**

Core	Maximum Soluble Boron (ppm)	Maximum Pin Power	Maximum Pin Discharge Burnup (GWD/MTM)
Equilibrium Cycle, Full MOX	1385	1.414	57.27
Initial Mixed Core	941	1.518	56.75
Scenario 1	1341	1.756	58.31
Scenario 2	750	1.460	59.52
Full LEU	750	1.446	53.05
Limit	1829	1.528	60.00

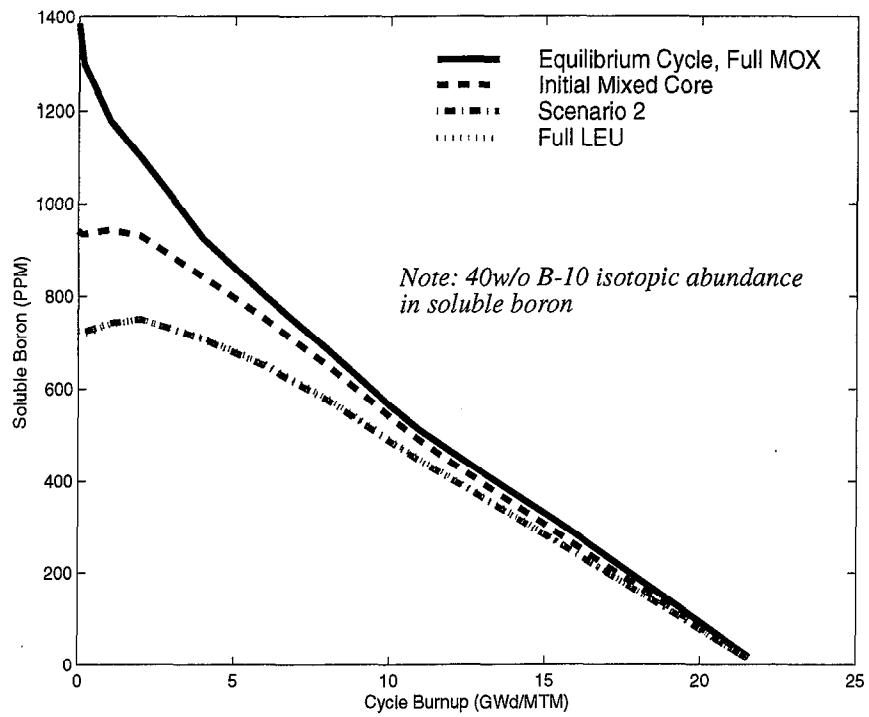


FIGURE 30. Soluble Boron Concentration vs. Cycle Burnup

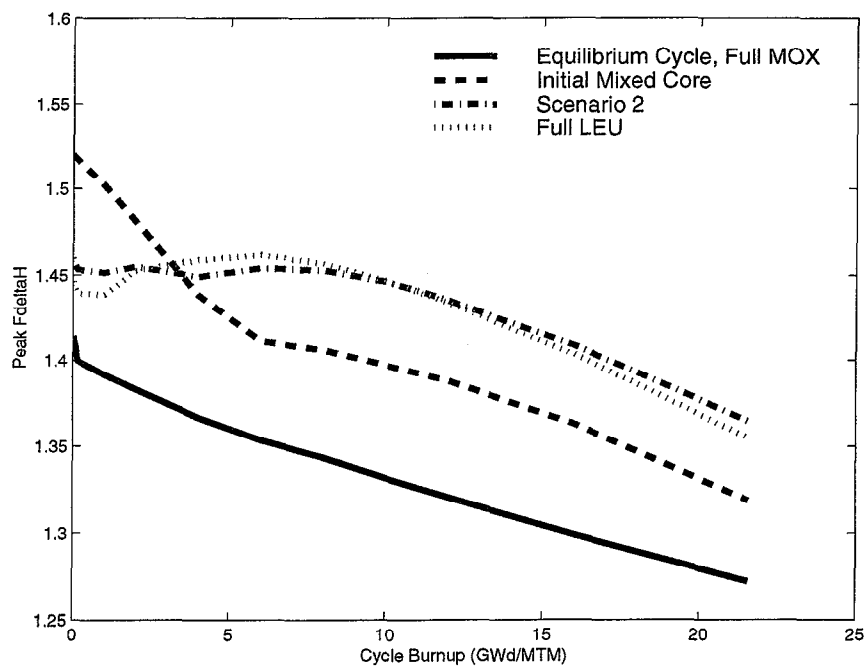
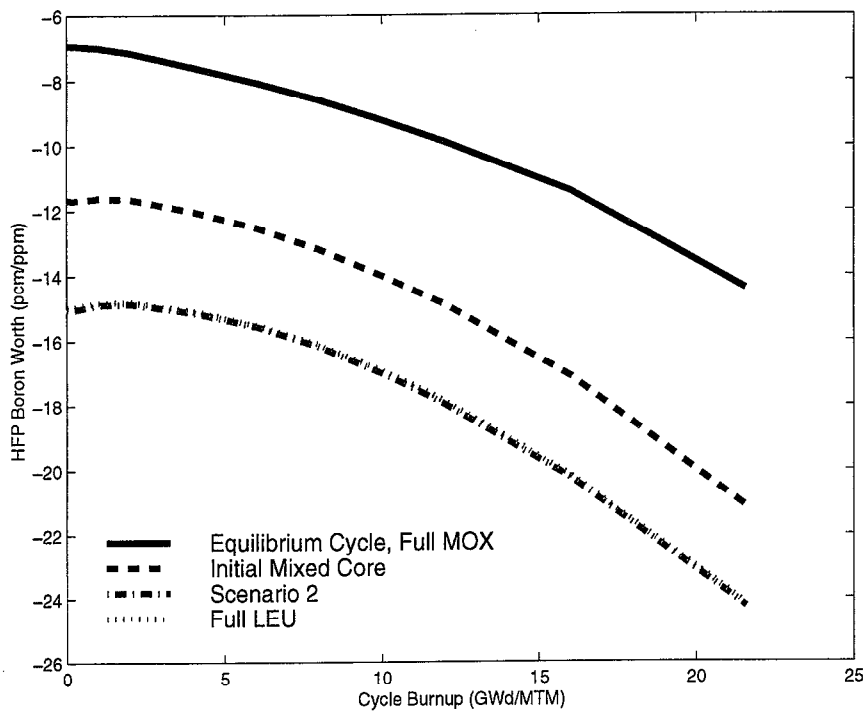
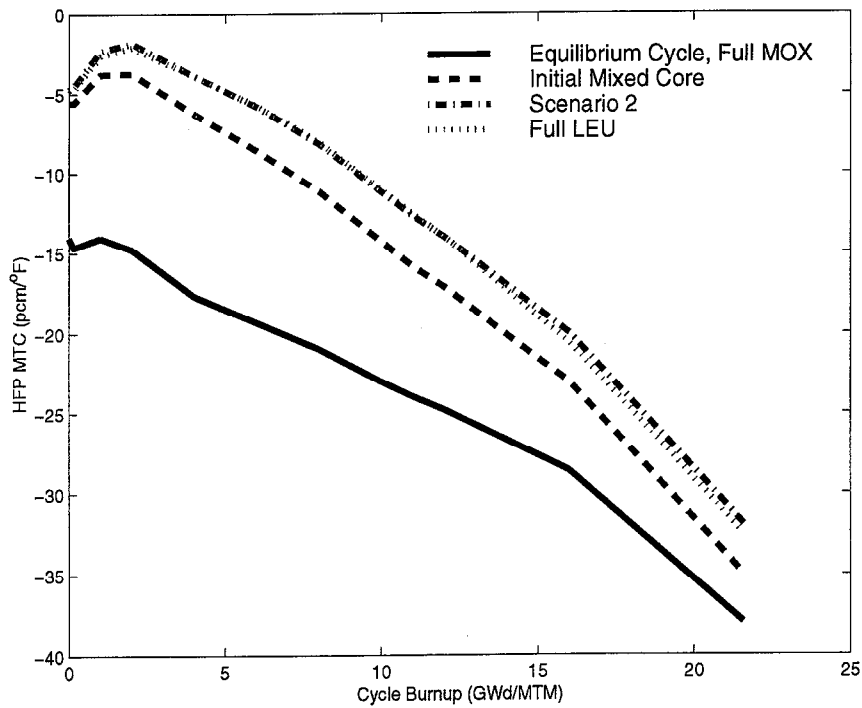


FIGURE 31. Peak  $F_{\Delta H}$  vs. Cycle Burnup



**FIGURE 32. HFP Boron Worth vs. Cycle Burnup**



**FIGURE 33. HFP MTC vs. Cycle Burnup**

## **7. Conclusions**

For the initial mixed LEU-MOX core, starting with the Westinghouse equilibrium cycle, full MOX core, an acceptable LP was determined in regard to satisfying all constraints. For the subsequent cycle, the following two disruption scenarios were examined: (1) complete availability of MOX feed assemblies and (2) complete unavailability of MOX feed assemblies.

The first scenario leads to a full MOX core. No LP could be determined which satisfied the maximum pin power constraint. Maximum pin power violations occur in almost all fresh MOX assemblies adjacent to burnt LEU assemblies. Modification of the lattice design, which was restricted in this study to uniform pin enrichments within an assembly as utilized in the equilibrium cycle, full MOX core, should be pursued to control the peak pin power by minimizing the adverse LEU-MOX assemblies interfacial effects.

The second scenario leads to a full LEU core. Transition cycles from an equilibrium cycle, full MOX core to a full LEU core have been developed. LPs found by FORMOSA-P for those transition cycles satisfy all constraints imposed.

## **8. Acknowledgment**

The authors would like to thank Dr. Trent Primm of Oak Ridge National Laboratory, Dr. Marvin Adams and Mr. Gustavo Alonso-Vargas of Texas A&M University, and Mr. Rick Ankney of Westinghouse Electric Company for their cooperation during the course of this study.

## **9. References**

- [1] "Plutonium Disposition Study: Implementation of Weapons Grade MOX Fuel in Existing Pressurized Water Reactors" Contract No. DE-AC03-93SF-19683, Westinghouse Electric Corporation (1996).
- [2] "FMS: The Scanpower Fuel Management System, HELIOS Documentation," Scanpower A/S (1995).
- [3] "FORMOSA-P V3.6.0 User's Manual: Fuel Management Optimization Software for PWRs," Electric Power Research Center, North Carolina State University (1998).

[4] "FORCIP-P Version 2.1 Code Manual: FORMOSA-P cross Section Interface Program," Electric Power Research Center, North Carolina State University (1998).

**INTERNAL DISTRIBUTION**

- |                    |                                       |
|--------------------|---------------------------------------|
| 1. M. D. DeHart    | 12. D. G. O'Connor                    |
| 2. R. J. Ellis     | 13-17. R. T. Primm, III               |
| 3. J. C. Gehin     | 18. C. C. Southmayd                   |
| 4. S. R. Greene    | 19-23. D. J. Spellman                 |
| 5. S. A. Hodge     | 24. R. M. Westfall                    |
| 6. D. T. Ingersoll | 25. K. A. Williams                    |
| 7. M. A. Kuliasha  | 26. B. A. Worley                      |
| 8. S. B. Ludwig    | 27. Central Research Library          |
| 9. G. E. Michaels  | 28. FMDP Library                      |
| 10. D. L. Moses    | 29-30. ORNL Laboratory Records (OSTI) |
| 11. B. D. Murphy   | 31. ORNL Laboratory Records-RC        |

**EXTERNAL DISTRIBUTION**

32. M. L. Adams, Department of Nuclear Engineering, Texas A&M University, Zachry 129, College Station, TX 77843
33. Dave Alberstein, LANL, P.O. Box 1663, MS-K575, Los Alamos, NM 87545
34. G. Alonszo, Department of Nuclear Engineering, P.O. Box 7909, North Carolina State University, Raleigh, NC 27695-7909
35. Richard D. Ankney, Westinghouse Electric Company, P.O. Box 355, Pittsburgh, PA 15230-0355
36. Imelda Ariani, Department of Nuclear Engineering, P.O. Box 7909, North Carolina State University, Raleigh, NC 27695-7909
37. Tim Barr, DOE, Chicago Operations Office, 9700 S. Cass Avenue, Chicago, IL 60439
38. H. R. Canter, Office of Fissile Materials Disposition, U.S. Department of Energy, MD-1/2, 1000 Independence Avenue SW, Washington DC 20585
39. G. S. Chang, INEEL, P.O. Box 1625, MS-3885, Idaho Falls, ID 83415-3885
40. A. I. Cygelman, Department of Energy, 1000 Independence Avenue SW, Forrestal Building 3F043, Washington, DC 20585
41. L. Groves, Sandia National Laboratories, P.O. Box 969, Livermore, CA 94551
42. D. Harrison, Department of Energy, 101 Convention Center Drive, Suite P200, Las Vegas, NV 89109
43. G. Holman, Lawrence Livermore National Laboratory, P.O. Box 808, Livermore, CA 94551
44. C. Jaeger, Sandia National Laboratories, P.O. Box 5800, Albuquerque, NM 78185-0759
45. Frank Motley, LANL, P.O. Box 1663, MS-K575, Los Alamos, NM 87545
- 46-50. Office of the ORNL Site Manager, Department of Energy, Oak Ridge National Laboratory, P.O. Box 2008, Oak Ridge, TN 37831
51. D. Peko, Department of Energy, 1000 Independence Avenue SW, Forrestal Building 3F042, Washington, DC 20585
52. P. T. Rhoads, Office of Fissile Materials Disposition, U.S. Department of Energy, MD-4, 1000 Independence Avenue SW, Washington, DC 20585
53. G. P. Rudy, Department of Energy, 1000 Independence Avenue SW, Forrestal Building 7B192, Washington, DC 20585
54. J. M. Ryskamp, INEEL, P.O. Box 1625, MS-3885, Idaho Falls, ID 83415-3885
55. Robert Selby, DOE, Chicago Operations Office, 9700 S. Cass Avenue, Chicago, IL 60439
56. J. Thompson, Office of Fissile Materials Disposition, U.S. Department of Energy, MD-4, 1000 Independence Avenue SW, Forrestal Building 3F043, Washington, DC 20585
57. Dr. Paul Turinsky, Department of Nuclear Engineering, North Carolina State University, Raleigh, NC 27695-7909